Propagation of polarized light in birefringent turbid media: time-resolved simulations

Xueding Wang and Lihong V. Wang

Optical Imaging Laboratory, Biomedical Engineering Program
Texas A&M University, 3120 TAMU, College Station, Texas 77843-3120
xwang@oilab.tamu.edu, lwang@tamu.edu

http://oilab.tamu.edu

Abstract: A Monte Carlo model was used to analyze the propagation of polarized light in linearly birefringent turbid media, such as fibrous tissues. Linearly and circularly polarized light sources were used to demonstrate the change of polarizations in turbid media with different birefringent parameters. Videos of spatially distributed polarization states of light backscattered from or propagating in birefringent media are presented.
© 2001 Optical Society of America

OCIS codes: (170.5280) Photon migration; (290.4210) Multiple scattering; (260.5430) Polarization; (290.7050) Turbid media; (290.4020) Mie theory

References and links

1. A. Ambirajan and D. C. Look, "A backward Monte Carlo study of the multiple scattering of a polarized laser beam," J. Quant. Spectrosc. Transfer **58**, 171–192(1997).
2. M. J. Rakovic, G. W. Kattawar, M. Mehrubeoglu, B. D. Cameron, L. V. Wang, S. Rastegar and G. L. Cote, "Light backscattering polarization patterns from turbid media: theory and experiment," Appl. Opt. **38**, 3399–3408(1999).
3. S. Bartel and A. H. Hielscher, "Monte Carlo simulations of the diffuse backscattering Mueller matrix for highly scattering media," Appl. Opt. **39**, 1580–1588(2000).
4. G. Yao and L. V. Wang, "Propagation of polarized light in turbid media: simulated animation sequences," Opt. Express **7**, 198–203 (2000). http://www.opticsexpress.org/oearchive/source/23140.htm.
5. J. F. de Boer, T. E. Milner, M. J. C. van Gemert and J. S. Nelson, "Two-dimensional birefringence imaging in biological tissue by polarization-sensitive optical coherence tomography," Opt. Lett. **22**, 934–936(1997).
6. M. J. Everett, K. Schoenenberger, B. W. Colston, Jr. and L. B. Da Silva, "Birefringence characterization of biological tissue by use of optical coherence tomography," Opt. Lett. **23**, 228–230(1998).
7. G. Yao and L. V. Wang, "Two-dimensional depth-resolved Mueller matrix characterization of biological tissue by optical coherence tomography," Opt. Lett. **24**, 537–539 (1999).
8. S. L. Jiao, G. Yao and L. V. Wang, "Depth-resolved two-dimensional Stokes vectors of backscattered light and Mueller matrices of biological tissue by optical coherence tomography," Appl. Opt. **39**, 6318–6324 (2000).
9. H. C. van de Hulst, *Light Scattering by Small Particles* (Dover, New York, 1981).
10. J. F. de Boer, T. E. Milner, and J. S. Nelson, "Determination of the depth-resolved Stokes parameters of light backscattered from turbid media by use of polarization-sensitive optical coherence tomography," Opt. Lett. **24**, 300–302 (1999).

1. Introduction

Recently, there has been increased interest in the propagation of polarized light in randomly scattering media because of its potential applications, especially in noninvasive optical diagnosis. In recent theoretical research, Ambirajan and Look [1] used a Monte Carlo technique to study the degree of polarization (DOP) of light diffusely reflected from turbid media. Rakovic *et al*. [2] and Bartel *et al*. [3] developed Monte Carlo algorithms to study the backscattered intensity patterns and compared their simulation results with experimental data. Yao and Wang [4] used a time-resolved Monte Carlo technique to present the propagation of polarized light in turbid media. Until now, all of these theoretical studies are limited to isotropic turbid media, which does not possess birefringence.

Birefringence is, however, prevalent in biological tissues, such as collagen or muscle. Tissue birefringence results primarily from the linear anisotropy of the fibrous structures that form the extra-cellular background medium. The refractive index of the background medium is higher along the length of fibers than that along the cross section. In birefringent turbid

media, both birefringence and scattering alters the polarization of light. Consequently, the birefringent effects of the background medium provide extraordinary information for subsurface imaging, which can be obtained by analyzing the diffusely reflected light [5–8]. This paper describes our study on the propagation of polarized light in birefringent turbid media based on a time-resolved Monte Carlo algorithm for the first time.

2. Monte Carlo algorithm for birefringent turbid media

Monte Carlo simulation to describe the multiple scattering events of photons in turbid media is based on radiative theory, which assumes that the scattering event is independent and has no coherence effects. The linearly birefringent tissue is looked on as a uniaxial material with the slow axis along the length of the fibers. The geometry of multiple scattering events in a birefringent turbid medium is shown in Fig. 1.
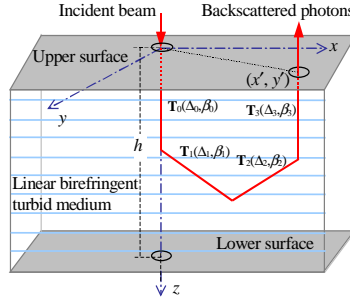

Fig. 1. Geometry of a multiple scattering event in a linearly birefringent turbid medium.

A photon is scattered in the background medium, which is anisotropic with the linear birefringent effect, by spherical particles then exits the medium from the surface of the sample. The cyan horizontal lines demonstrate the direction of the slow axis of the medium background, which is along the x-axis. The basic Stokes-Mueller formalism for tracing the propagation of each polarized photon packet in turbid media has been described in Refs. [2–4]. Considering the birefringence of the media, we express the Stokes vector of a diffusely reflected photon packet after it has been scattered n times in a birefringent turbid medium as

$$\mathbf{S}_n^{bs}(x', y'; \mu_s, \mu_a, \delta) = [\mu_s / (\mu_a + \mu_s)]^n \times \mathbf{R}(\phi_n)\mathbf{T}(\Delta_n, \beta_n)\mathbf{M}(\Theta_n)\mathbf{R}(\phi_{n-1\ n})...$$

$$\times \mathbf{T}(\Delta_2, \beta_2)\mathbf{M}(\Theta_2)\mathbf{R}(\phi_{1\ 2})\mathbf{T}(\Delta_1, \beta_1)\mathbf{M}(\Theta_1)\mathbf{R}(\phi_1)\mathbf{T}(\Delta_0, \beta_0)\mathbf{S}_0, \quad (1)$$

where μ_s, μ_a are the scattering and absorption coefficients, respectively; δ is the linear birefringence value; (x', y') is the detection point on the upper surface of the turbid medium in the laboratory coordinate. $\mathbf{S}_0$ and $\mathbf{S}_n^{bs}$ represent the Stokes vectors of the incident and the backscattered photons, respectively. $[\mu_s / (\mu_a + \mu_s)]^n$ expresses the remaining energy after the photon has been scattered n times. $\mathbf{R}(\phi)$ is the rotation matrix that connects the two Stokes vectors that describe the same polarization state but with respect to the two reference planes such that one reference plane coincides with the other after a counterclockwise rotation by angle ϕ around the direction of light propagation [2]. $\mathbf{M}(\Theta)$ is the matrix for each single scattering event based on Mie theory [9], where Θ is the scattering angle. $\mathbf{T}(\Delta, \beta)$ describes the birefringent effect on the photon packet in each free path, which can be expressed as

$$\mathbf{T}(\Delta, \beta) = \begin{bmatrix} 1 & 0 & 0 & 0 \\ 0 & C_4 \sin^2(\Delta/2) + \cos^2(\Delta/2) & S_4 \sin^2(\Delta/2) & -S_2 \sin(\Delta) \\ 0 & S_4 \sin^2(\Delta/2) & -C_4 \sin^2(\Delta/2) + \cos^2(\Delta/2) & C_2 \sin(\Delta) \\ 0 & S_2 \sin(\Delta) & -C_2 \sin(\Delta) & \cos(\Delta) \end{bmatrix},$$

$$C_2 = \cos(2\beta), C_4 = \cos(4\beta), S_2 = \sin(2\beta), S_4 = \sin(4\beta). \quad (2)$$

β is the azimuthal angle of the birefringent slow axis at the *x-y* plane in the local coordinate of the propagating photon. Δ is the phase retardation, which can be obtained by

$$\Delta = (\Delta n) \times 2\pi s / \lambda , \qquad (3)$$

where *s* is the step length; λ is the wavelength of the light *in vacuo*; and Δn is the difference between the maximum and minimum refractive indices in the plane perpendicular to the propagation orientation of the photon packet. When the angle α between the slow axis of the medium and the propagation orientation of the photon packet is known, Δn can be shown as

$$\Delta n = n_s n_f / \sqrt{(n_s \cos\alpha)^2 + (n_f \sin\alpha)^2} - n_f . \qquad (4)$$

n_s and n_f are the refractive indices of the birefringent medium along the slow axis and the fast axis, respectively; the linear birefringence value δ is n_s–n_f.

3. Results

For comparison, we kept most parameters of the light and the turbid media constant in following simulations and altered only the polarization states of the incident light and the parameters of birefringence. λ is 594 nm. The radius of the spherical scattering particles in the media is 350 nm. The refractive index of the scattering particles is 1.57. n_s is 1.33. The anisotropic factor *g* is calculated to be 0.9. μ_s and μ_a are 90 cm^{-1} and 1 cm^{-1}, respectively.

3.1 Polarization of light backscattered from birefringent turbid media

The DOLP (degree of linear polarization) patterns of backscattered light from isotropic and birefringent turbid media for linear incident polarization are shown in Fig. 2. When the incident light is right-circularly polarized, the comparison of the DOCP (degree of circular polarization) patterns is shown in Fig. 3. For both figures, δ is $1.33/1000$. Every picture in Figs. 2 and 3 is centered at the point of incidence. The actual size of each picture is 1×1 mm^2.

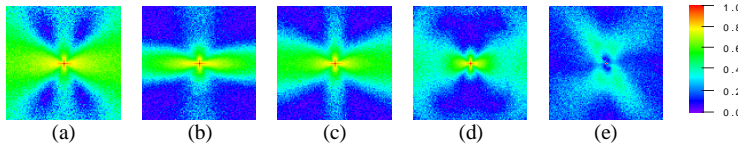(a)   (b)   (c)   (d)   (e)

Fig. 2. DOLP patterns of backscattered light from (a) an isotropic turbid medium and (b)–(e) birefringent turbid media. The incident light is linearly polarized with the polarization oriented at the *x*-axis. Orientations of the birefringent slow axes of the turbid media are along the *x*-axis, *y*-axis, *z*-axis, and 45° in the *x-y* plane for the results in (b) to (e), respectively.

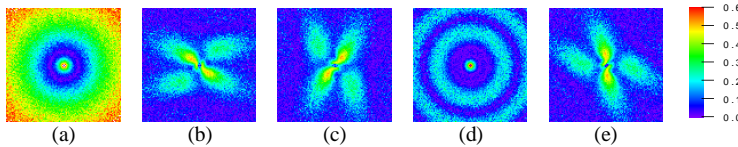(a)   (b)   (c)   (d)   (e)

Fig. 3. DOCP patterns of backscattered light from (a) an isotropic turbid medium and (b)–(e) birefringent turbid media. The incident light is right-circularly polarized. Orientations of the birefringent slow axes of the turbid media are along the *x*-axis, *y*-axis, *z*-axis, and 45° in the *x-y* plane for the results in (b) to (e), respectively.

When light propagates in the birefringent turbid media, the change of polarization depends on the orientations and the lengths of the discontinuous paths of the photon as well as the orientation of the birefringence in the medium, which has been shown in Eqs. 2–4. The statistic distribution of the changes of polarization in the turbid medium can be observed from the spatial polarization patterns of the backscattered light. The symmetries in the patterns can be explained by the symmetries in the single scattering matrix, the orientation of birefringence

and the polarization state of the incident light. For instance, in the birefringent turbid media, the circularly polarized light no longer product a uniform distribution in the dimension of the azimuthal angle in the single scattering event; therefore, for circularly polarized incident light, the polarization patterns of the backscattered light do not have to be rotationally symmetric but depend on the orientation of the birefringence in the medium.

It is noticeable that when the light is circularly polarized and the orientation of the birefringent slow axis is along the z-axis, detected DOCP of backscattered light drops with oscillation when the source-detector distance increases (Fig. 4). The oscillation is correlated with the periodic phase retardation caused by the birefringence.
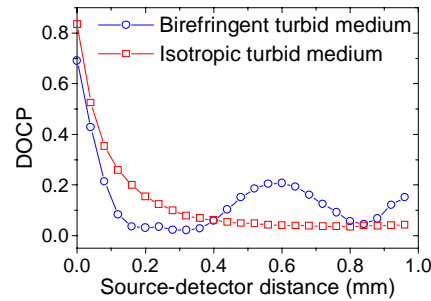

Fig. 4. DOCP of backscattered light vs. the source-detector distance. Incident light is right-circularly polarized. The blue circles are the results for the birefringent turbid medium with the slow axis oriented along the z-axis in the laboratory coordinate; the red squares are the results for an isotropic turbid medium for comparison.

Figures 5(a) shows the time-resolved DOLP of backscattered light from the birefringent turbid media with the birefringent slow axes oriented along the 45° in the x-y plane, where the incident light is linearly polarized along the x-axis. The linear birefringence value δ is set to be $1.33/1000$ and $1.33 \times 2/1000$, respectively. For right-circularly polarized incident light, the time-resolved DOCP of backscattered light from the birefringent turbid media with the birefringent slow axes oriented along the cross section of the z-axis is shown in Fig. 5(b). The period of the oscillations in Fig. 5 is inversely proportional to δ. In isotropic scattering media, the DOLP and DOCP of backscattered light decrease when the time of propagation increases, because multiply scattered photons usually have greater path length than weakly scattered photons. However, in birefringent scattering media, the DOLP and DOCP present oscillations as a function of time because of the periodic phase retardation caused by the birefringence, a similar phenomenon was observed in optical-coherence tomography [10].
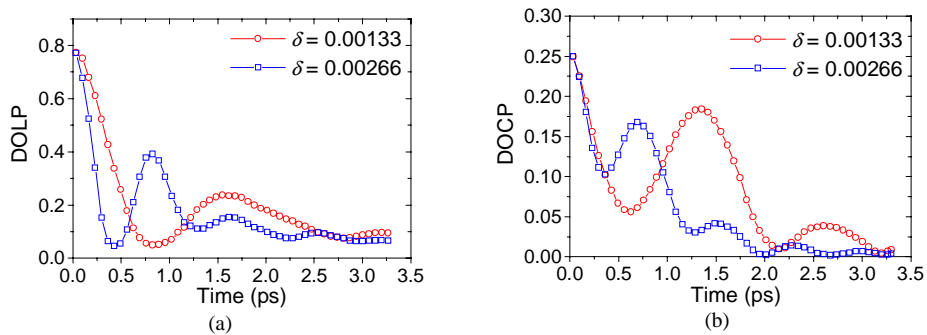

Fig. 5. (a) Time-resolved DOLP of backscattered light from birefringent turbid media with the slow axes oriented along the 45° in the x-y plane. Incident light is linearly polarized with the polarization oriented at the x-axis. (b) Time-resolved DOCP of backscattered light from birefringent turbid media with the slow axes oriented along the cross section of z-axis. Incident light is right-circularly polarized.

Videos of the polarizations of the backscattered light from an isotropic turbid medium and birefringent turbid media with different orientations of slow axis are shown in Figs. 6 and 7 for linear and circular incident polarizations, respectively. The propagation time of photons changes from 0 to 3.3 ps. The actual size of each video sequence is 1×1 mm^2. These videos demonstrate how the polarization states of the diffusely reflected light depend on the propagation time as well as the birefringence in the turbid media.
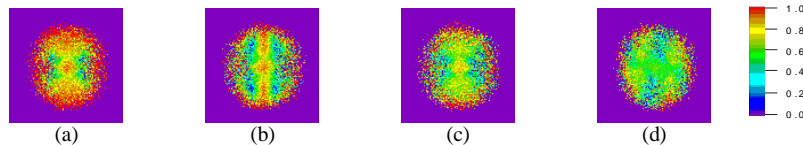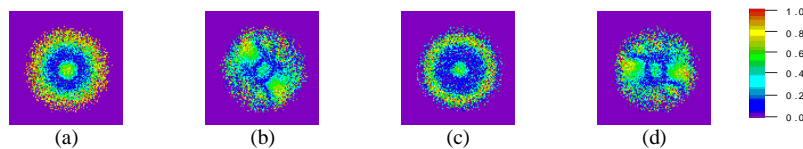

| (a) | (b) | (c) | (d) |

Fig. 6. (880 KB) Videos of the DOLP of the backscattered light from (a) an isotropic turbid medium and (b)–(d) birefringent turbid media with the slow axes oriented along the *x*-axis, *z*-axis and 45° angle in the *x*-*y* plane, respectively. Incident light is linearly polarized with the polarization oriented at the *x*-axis.

| (a) | (b) | (c) | (d) |

Fig. 7. (880 KB) Videos of the DOCP of the backscattered light from (a) an isotropic turbid medium and (b)–(d) birefringent turbid media with the slow axes oriented along the *x*-axis, *z*-axis and 45° angle in the *x*-*y* plane, respectively. Incident light is right-circularly polarized.

3.2 Polarization propagation in single-layer birefringent turbid media

In order to demonstrate the linearly birefringent effect on polarized light in detail, we present videos of polarization propagations in birefringent turbid media with different orientations of slow axis, as shown in Figs. 8 and 9 for linear or circular incident polarizations, respectively. Fig. 8(a) and Fig. 9(a) show the results for an isotropic medium for comparison. These two-dimensional sequences represent the three-dimensional distributions of the polarizations projected onto the *x*-*z* plane in the laboratory coordinate. The actual size of each video sequence is 1×2 mm^2. The polarization states of the photons at the expanding edges are retained well in the isotropic turbid medium because the photons there experience very few scattering events. However, in the birefringent turbid media, the polarization states at the expanding edges depend on the geometric positions of the edges in the media, the orientation of the birefringence in the media and the incident polarization state, though the DOP of the light at the expanding edges is retained well. The alternate and periodic changes between the circular and linear polarization states of the light at the expanding edges are caused by the periodic phase retardation in the birefringent media.
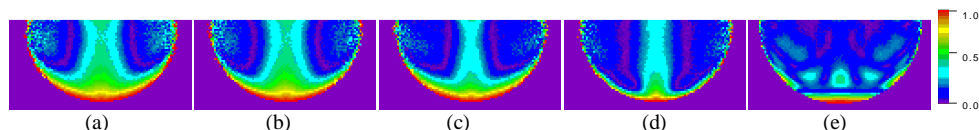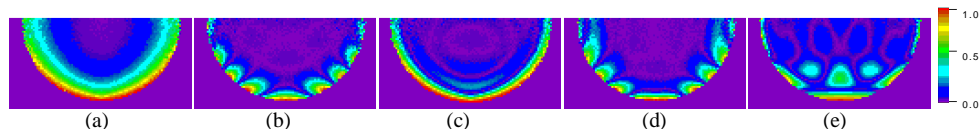

| (a) | (b) | (c) | (d) | (e) |

Fig. 8. (2,462 KB) Videos of the DOLP propagations in (a) an isotropic turbid medium and (b)–(e) birefringent turbid media with the slow axes oriented along the *x*-axis, *y*-axis, *z*-axis and 45° angle in the *x*-*y* plane, respectively. Incident light is linearly polarized with the polarization oriented at the *x*-axis.

| (a) | (b) | (c) | (d) | (e) |

Fig. 9. (2,462 KB) Videos of the DOCP propagations in (a) an isotropic turbid medium and (b)–(e) birefringent turbid media with the slow axes oriented along the *x*-axis, *y*-axis, *z*-axis and 45° angle in the *x*-*y* plane, respectively. Incident light is right-circularly polarized.

3.3 Polarization propagation in two-layer birefringent turbid media

In actual biological tissues, for example human skin, the orientations of the fibrous structures vary in different layers. In this case, the propagation of polarized light is much more complicated, because the birefringence with different orientations and δ in each layer has a combined effect on the polarization propagation of light in the medium.

We studied the polarization propagation in a two-layer turbid medium. The orientations of the birefringent slow axes in the upper and lower layer are along the *y*-axis and *x*-axis, respectively. The two layers have the same birefringent value δ that equals $1.33/1000$. The thicknesses of the upper and lower layers are 0.4 mm and 0.6 mm, respectively. Videos of DOP, DOLP and DOCP in this two-layer birefringent turbid medium for different incident polarizations (the linear polarization oriented at *x*-axis and the right-circular polarization) are shown in Figs. 10 and 11, respectively. The gray dot lines in pictures show the interface of the two layers. The actual size of each video sequence is 1×2 mm^2. It is noticeable that the polarization patterns are different at the upper and lower sides of the two-layer interface because of the different orientations of the birefringence in the two layers.

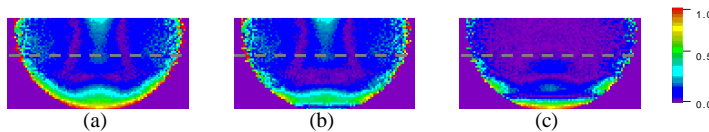   (a)   (b)   (c)

Fig. 10. (1,935 KB) Videos of the (a) DOP, (b) DOLP and (c) DOCP propagations in a turbid medium with a two-layer structure. The upper layer is a birefringent turbid medium with the slow axis oriented along the *y*-axis; the thickness is 0.4 mm; the lower layer is a birefringent turbid medium with the slow axis oriented along the *x*-axis; the thickness is 0.6 mm. Incident light is linearly polarized with the polarization oriented along the *x*-axis.
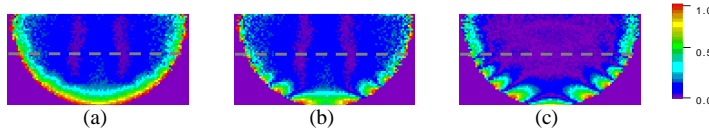

    (a)   (b)   (c)

Fig. 11. (1,935 KB) Videos of the (a) DOP, (b) DOLP and (c) DOCP propagations in a turbid medium with a two-layer structure. The upper layer is a birefringent turbid medium with the slow axis oriented along the *y*-axis; the thickness is 0.4 mm; the lower layer is a birefringent turbid medium with the slow axis oriented along the *x*-axis; the thickness is 0.6 mm. Incident light is right-circularly polarized.

4. Conclusion

We theoretically studied the propagations of polarized light in birefringent turbid media based on a time-resolved Monte Carlo algorithm. The polarization patterns of backscattered light and the spatially distributed polarization states in the birefringent turbid media were analyzed. Linearly polarized light and circularly polarized light were considered as sources. Results for media with different birefringent parameters including the orientation of fibers and the birefringence value δ were compared and discussed.

The theoretic study presented in this paper should contribute to the understanding of the essential physical processes of polarized light propagation in birefringent tissues. The Monte Carlo simulation cannot model coherent phenomena of tissue optics, however this method can be applied in the non-coherent regime or in cases where coherent effects are removed. Some phenomena observed in the simulation can provide potential methods for use in actual subsurface tomography of fibrous tissues.